05

Heating of a metal layer by a scanning laser beam

© V. Trofimov[1], Pengcheng Lin[1], S.V. Fedorov[2,¶], N.N. Rosanov[2], N.A. Veretenov [2], Yan Wang[1], Yongqiang Yang[1]

[1] South China University of Technology, 510640 Guangzhou, China
[2] Ioffe Institute, St. Petersburg, Russia

[¶] e-mail: sfedorov2006@bk.ru

Received December 20, 2022
Revised December 20, 2022
Accepted January 09, 2023.

The analysis and numerical simulation of the heating mode of a metal plate scanning beam of laser radiation was carried out. In the transverse-one-dimensional approximation, the estimates are obtained of the main dependences of the characteristics of the steady temperature profile on the parameters of the problem..

Keywords: Laser heating of metal, laser beam scanning, temperature profile.

DOI: 10.61011/EOS.2023.03.56188.92-23

Introduction

An actively developing application of lasers is 3D - printing based on the effects of laser radiation on metals, plastics and other substances [1–8]. The substance (later, metal is considered) is heated by a laser beam scanning over the sample surface. The scanning mode largely determines the quality of manufactured samples, and therefore, the scanning influence and the choice of its strategy have been widely studied in the literature (see, for example, [9–18]). It should be noted that in practice, there is always some spatial gap between scanning lines. It also affects the quality of the fabricated sample, since the required temperature for metal melting in this area is achieved through thermal conduction, since this area may not be sufficiently illuminated by the laser beam. The choice of the distance between the scanning lines also depends on the scanning speed, with an increase in which, the effective heating area of the medium along the scanning direction is determined not only by the beam radius, but also by the scanning speed. This, in turn, affects the thermal conductivity both along the scanning direction and perpendicular to it. Finally, the metal heating for its subsequent melting is also determined by the sample thickness and the heat exchange with the environment and the substrate. As the latter in 3D - printing systems, the „plate“ on which the product is shaped can be used. Thus, trend identification and assessment of the temperature profile parameters of the heated metal depending on the factors listed above (scanning speed, sample thickness (powder or plate) of the metal, beam radius, optical radiation power) would allow to optimize the heating and facilitate the scanning strategy choice. This is the problem this paper is devoted to.

The paper is organized as follows. In the following section, we introduce the model and formulate the basic heat conduction equation for the temperature averaged over the metal plate thickness. Next, the transition to dimensionless parameters is made, and the asymptotics of the temperature distribution away from the scanning laser beam is determined. Then, the temperature setting time is assessed for constant-speed scanning, and the important role of the plate structure is revealed — whether it is a solid metal or a layer of metal balls. The shift of the temperature maximum relative to the maximum of the laser beam intensity is also assessed, and the widths of the front and back fronts of the temperature profile are estimated. The heat conduction equations obtained by numerical solution, the basic dependences of the steady-state temperature profile characteristics on the task parameters are presented. The main conclusions are summarized in the Conclusion.

Model and basic relations

The initial thermal conductivity equation describing the metal plate heating has the form

$$C_V \frac{\partial T}{\partial t} = \frac{\partial}{\partial x}\left(\kappa(T)\frac{\partial T}{\partial x}\right) + \frac{\partial}{\partial y}\left(\kappa(T)\frac{\partial T}{\partial y}\right) + \frac{\partial}{\partial z}\left(\kappa(T)\frac{\partial T}{\partial z}\right) + w_v. \quad (1)$$

Here, T — temperature, t — time, C_V — specific heat capacity at constant volume, κ — thermal conductivity coefficient and w_v — heat release density due to absorption of laser radiation falling on the plate approximately along the normal. We assume that the temperature does not exceed the metal melting point, so that no - hydrodynamic effects occur in the metal. The plate thickness L is located between the gas temperature T_g at $z > 0$ and the fixed temperature T_{sub} substrate at $z < -L$ (Fig. 1). The laser radiation falls on the plate from the gas medium and is reflected with a reflectance R, which depends on the

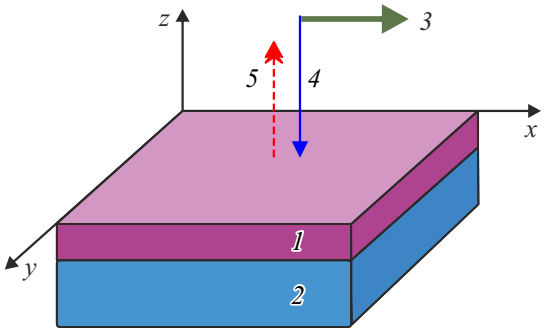

Figure 1. Modelling details. *1* — the metal layer to be machined, *2* — the substrate.*3* — laser beam moving *4* in the direction x (3) with speed V.*5* — the heat flux from the heated metal.

temperature T. On the faces of the plate $z = 0$ and $z = L$, the heat fluxes are described by Newton's law

$$\kappa \frac{\partial T}{\partial z}\bigg|_{z=0} = \alpha_g (T - T_g),$$

$$\kappa \frac{\partial T}{\partial z}\bigg|_{z=-L} = -\alpha_{\text{sub}} (T - T_{\text{sub}}). \qquad (2)$$

In (2), $\alpha_{g,\text{sub}}$ — heat transfer coefficients on the corresponding faces. Below, we will complete the heat transfer description by taking into account the radiation heat transfer.

Under characteristic conditions, the temperature difference T_g and T_{sub} is small, and the plate is so thin (condition $L \ll \kappa/\alpha_{\text{sub}}$), that its temperature changes little in the normal direction. Then, one can use the mean field approximation, i.e., averaging the thermal conductivity equation over z, as is performed in optical bistability problems with a thermal nonlinearity mechanism [19,20]. In this case, in addition to reducing the geometric dimension of the problem, the boundary conditions (2) are taken into account by the averaged equation itself. For a metal plate, the laser radiation is completely absorbed at its thickness; then, the average heat emission is $\langle w_v \rangle = \frac{1}{L} \int\limits_0^L w_v dz = BI_{\text{in}}$, where $B = \frac{1}{L}(1 - R)$. As a result, we obtain a closed reduced heat equation describing the dynamics of the averaged temperature $\langle T \rangle = \frac{1}{L} \int\limits_0^L T dz$ (we omit the averaging sign below):

$$C_V(T) \frac{\partial T}{\partial t} = \frac{\partial}{\partial x}\left(\kappa(T) \frac{\partial T}{\partial x}\right) + \frac{\partial}{\partial y}\left(\kappa(T) \frac{\partial T}{\partial y}\right) - \Phi(T) + B(T) I_{\text{in}}. \qquad (3)$$

In (3) x and y — transverse coordinates, I_{in} — incident laser beam intensity at $z = 0$ and

$$\Phi(T) = \frac{1}{L}\left[\alpha_{\text{sub}}(T - T_{\text{sub}}) + \alpha_g (T - T_g) + \alpha_R (T^4 - T_g^4)\right]. \qquad (4)$$

Here, α_R — radiation heat transfer coefficient at the gas boundary. The substrate is considered thick enough (ideally, semi-infinite). If there is no substrate, its thermo-physical characteristics are replaced in (4) by those of the surrounding gas. In the absence of laser heating or away from the laser beam, the steady state (averaged over z) temperature of the plate T_0 is determined by the condition $\Phi(T_0) = 0$. The dimensions of the thermo-physical parameters are as follows: $[C_V] = \text{W} \cdot \text{s} \cdot \text{m}^{-3} \cdot \text{K}^{-1}$, $[\kappa] = \text{W} \cdot \text{s} \cdot \text{m}^{-3} \cdot \text{K}^{-1}$, $[\alpha_g] = [\alpha_{\text{sub}}] = \text{W} \cdot \text{m}^{-2} \cdot \text{K}^{-1}$, $[\alpha_R] = \text{W} \cdot \text{m}^{-2} \cdot \text{K}^{-4}$.

Next, we consider the laser beam scanning mode along the surface at constant speed V along the axis x, without affecting the temperature dependence on another transverse coordinate y; for a small-sized metal beam in the direction y, averaging is also realized along this direction. Then, there is no $\frac{\partial}{\partial y}\left(\kappa(T) \frac{\partial T}{\partial y}\right)$ term in (3), and the radiation intensity depends on only one combined variable: $I_{\text{in}} = I_{\text{in}}(x - Vt)$. Introducing $X = x - Vt$, in steady-state mode, we get

$$\frac{d}{dX}\left(\kappa(T) \frac{dT}{dX}\right) + VC_V(T) \frac{dT}{dX} - \Phi(T) + B(T) I_{\text{in}}(X) = 0. \qquad (5)$$

This equation determines the steady-state temperature profile. The unsteady equation also allows us to describe the process of its establishment. Next, for certainty, we consider $V > 0$.

The temperature dependences of the thermo-physical characteristics and the reflectance are set by the metal parameters. For copper, they are given in the Appendix based on data [21–24].

Dimensionless variables and dimensionless heat conduction equation

The dimensionless form of the governing equations allows us to scale solutions and use the results of a single numerical calculation to obtain information about many variants of the problem parameters. For this purpose, we introduce the operating temperature and dimensionless thermo-physical parameters, highlighting their values at the operating temperature: $c_v = C_V(T)/C_{V,N}$, where$C_{V,N} = C_V(T_{\text{work}})$, and similarly $\Lambda = \kappa(T)/\kappa_N$, $\beta_g = \alpha_g(T)/\alpha_{g,N}$, $\beta_{\text{sub}} = \alpha_{\text{sub}}(T)/\alpha_{\text{sub},N}$, and $\beta_R = \alpha_R(T)/\alpha_{R,N}$. Then, we introduce the time scale

$$\tau_0 = (C_{V,N}/\alpha_{g,N})L \qquad (6)$$

and dimensionless time $\tau = t/\tau_0$. The time $\tau_0(T_{\text{work}})$ serves as a natural estimate of the stationary mode establishment time. The natural scale of the coordinate is $L_{\text{scale}} = (L \cdot \kappa_N/\alpha_{g,N})^{1/2}$, so the dimensionless coordinate $\xi = x/L_{\text{scale}}$. It is convenient to enter the dimensionless scanning speed by the ratio $v_s = lV/V_{\text{scale}}$, where $V_{\text{scale}} = L/\tau_0 = \alpha_{g,N}/C_{V,N}$ and

$l = L/L_{\text{scale}} = [L/(\kappa_N/\alpha_{g,N})]^{1/2}$. The dimensional temperature T will be represented as $T = T_0 = \Theta T_{\text{work}}$, where $\Theta = (T - T_0)/T_{\text{work}}$ — deviation of the relative temperature from the equilibrium value in the absence of laser radiation. Finally, the dimensionless laser intensity $I_0 = I_{\text{in}}/(\alpha_{g,N} T_{\text{work}})$. Although we are considering a one-dimensional problem here, we will assume that the laser beam — is an axisymmetric spot when calculating the real laser power.

In dimensionless form, the heat conduction equation is written as

$$C_V(\Theta)\frac{\partial\Theta}{\partial\tau} = \frac{\partial}{\partial\tau}\left(\Lambda\frac{\partial\Theta}{\partial\xi}\right) - \varphi(\Theta) + [1 - R(\Theta)]I_0, \quad (7)$$

where

$$\varphi(\Theta) = \beta_g(\Theta - \Theta_g) + \frac{\alpha_{\text{sub},N}}{\alpha_{g,N}}\beta_{\text{sub}}(\Theta - \Theta_{\text{sub}}) + \frac{\alpha_{r,N}}{\alpha_{g,N}} T_{\text{work}}^3 \beta_R \left[\left(\Theta + \frac{T_0}{T_{\text{work}}}\right)^4 - \left(\frac{T_g}{T_{\text{work}}}\right)^4\right] \quad (8)$$

and $\Theta_g = (T_g - T_0)/T_{\text{work}}$, $\Theta_{\text{sub}} = (T_{\text{sub}} - T_0)/T_{\text{work}}$.

The ratio $\Phi(T_0 = 0)$ changes to the condition $\varphi(0) = 0$.

In case of constant-speed laser beam scanning, the intensity is $I_0 = I_0(\chi)$, where $\chi = \xi - v_s\tau$. In the steady-state mode $\Theta = \Theta(\chi)$, so that the steady-state temperature profile is defined by the ordinary differential equation

$$\Lambda(\Theta)\frac{d^2\Theta}{d\chi^2} + K(\Theta)\left(\frac{d\Theta}{d\chi}\right)^2 + v_s c_v \frac{d\Theta}{d\chi} - \varphi(\Theta) + \big[1 - R(\Theta)\big]I_0(\chi) = 0, \quad (9)$$

where $K = d\Lambda/d\Theta$, with boundary conditions $\Theta_{\chi\to\pm\infty} = 0$.

At the beam periphery, the laser intensity is negligibly low. There, the metal temperature differs little from the equilibrium temperature, and its approach to the equilibrium value has an exponential character, $\Theta \sim \exp(\gamma\chi)$. The exponent index γ is determined from the equation (9) linearized near the equilibrium temperature value:

$$\Lambda_0\gamma^2 + v_s c_{v,0}\gamma - \varphi_0' = 0, \quad (10)$$

where $\Lambda_0 = \Lambda(0)$, $c_{v,0} = c_v(0)$, $\varphi_0' = (d\varphi/d\Theta)_{\theta=0}$.

The solution of the quadratic equation (10) under characteristic conditions ($\Lambda(0) > 0$, $c_{v,0} > 0$, $\varphi_0' > 0$) are two real roots opposite in sign

$$\gamma_\pm = \frac{1}{2\Lambda_0}\left[-v_s c_{v,0} \pm \sqrt{(v_s c_{v,0})^2 + 4\Lambda_0\varphi_0'}\right]. \quad (11)$$

Accordingly, the front temperature profile has a characteristic width of $1/|\gamma_-|$, and the width of the rear front $\sim 1/|\gamma_+|$. Naturally, the leading front width is less than that of the rear. The difference in the widths of the fronts means the temperature profile asymmetry when heated even by a symmetrical (with color-shaped intensity distribution) laser beam and leads to a temperature maximum shift relative to the maximum intensity of the laser beam. Assessments show that for small thicknesses of the metal layer, this shift increases approximately linearly with the scanning speed. The numerical calculation below gives more complete information. Note also that a comparison with heating with homogeneous laser radiation (the limit of infinitely large beam width) gives a useful estimate from below of the laser beam intensity needed to heat the metal to a given temperature T_m. With this heating, the temperature is also homogeneous, and the laser intensity is determined by the ratio $I_{\text{hom}} = \varphi(\Theta_m)/[1 - R(\Theta_m)]$. Naturally, for a finite width beam, the maximum intensity shall exceed the value I_{hom}. Next, using numerical calculations using the thermo-physical parameters of the metal, we give quantitative data on the temperature profile.

Assessments of the temperature profile establishment time and ball model

The formula (6) for the time of establishing the temperature profile testifies to its proportionality to the metal layer thickness. For volumetric copper parameters (see Appendix), we obtain very large values for the setting time by (6): $\tau_0 = 4.15 \cdot 10^4$ s $= 11.5$ hour for $L = 0.1\,m$ and $\tau_0 = 4.15$ s for $L = 10\,\mu$m. In reality, the metal in the problem under consideration is not solid, but consists of micron-sized balls. This leads to a reduction in density and an increase in the effective surface area of the metal. Let the density decrease to two times of - for the geometric factor, and the specific heat capacity — proportional to the ratio of the total surface balls area to its part concerning the other balls (up to twenty times), so that further in determining dimensional constants we can substitute $C_V \to C_V/c_{V\text{eff}}$, still considering that C_V — the heat capacity density of bulk copper. In addition, the convection and radiation cooling coefficients α_g and α_R increase in proportion to the ratio of the total surface area of all balls in a plate of thickness L to the surface area of a solid copper plate, for example $\alpha_g \to c_{Sph}\alpha_g$ and $c_{Sph} = 20$. The indicated substitutions affect only the normalization of the parameters: setting time τ_0, scaling of the scanning speed and the beam intensity. Further, we assume that the reduction factor for the cooling/heating time of the balls compared to a whole plate is $c_{\tau\text{eff}} = c_{V\text{eff}}c_{Sph} = 400$, so that the characteristic setting time for copper balls $\tau_0 \approx 10^{-2}$ s for $L = 10\,\mu$ m. Similarly, replacing the solid metal with balls increases the heat transfer to the substrate; for the steel substrate, this reduction is estimated to be up to 10 fold. Thus, the temperature setting time can be small for a thin layer of balls. Further results are given for already established temperature profiles.

Shift of the maximum temperature profile relative to the laser intensity profile

We will assume that the laser beam intensity profile is bell-shaped, with one maximum at $\chi = 0$, and $I_0(0) = I_m$. The maximum of the stationary temperature profile will be shifted toward the rear front, so that the maximum temperature $\Theta = \Theta_{\max}$ is reached at $\chi = \chi_{\max} < 0$. By decomposing the temperature profile into a series of small deviations from $\chi_{\max}$ up to the cubic terms, the following inequalities can be obtained:

$$0 < I_0'(\chi_{\max}) < v_s \frac{\Theta_{\max} - \Theta_m}{\Theta_m} \frac{c_\rho(\Theta_m)\varphi(\Theta_m)}{1 - R(\Theta_m)}. \qquad (12)$$

When the upper constraint (12) is converted into equality in the limiting cases of „thin“ and „thick“ metal layer, we obtain for shift $\chi_{\max}$with respect to the dimensionless beam width ρ_b

$$\chi_m/\rho_b \approx \begin{cases} -\frac{1}{2}\rho_b(1 - I_{\text{hom}}/I_m)(V/V_{\text{scale}})/l, & (V/V_{\text{scale}})l \ll 1, \\ -\ln^{1/2}(I_{\text{hom}}/I_m), & (V/V_{\text{scale}})l \gg 1. \end{cases} \qquad (13)$$

In Fig. 2, for a beam with a characteristic dimensionless width („radius“) ρ_b, the dependence $\chi_{\max}$ on $I_{\max} = I_{\text{in}}(0)$, such that the upper constraint (12) turns into an equality. At the same time, as the intensity $I_{\max}$ changes, the beam width ρ_b also changes so that the power is constant. The figure is given for the case of a thin layer of balls with thickness $L = 10\,\mu$m. The main difference between the „thin“ layer and the „thick“ layer is that the relative deviation decreases by about 100 fold, which is consistent with the assessments (13).

Width assessments of the temperature profile fronts for a layer of copper

Let us estimate the front widths based on relation (11) for a thin copper layer at laser beam scanning speeds $V = 5 \ldots 10$ cm/s. In this case, it turns out that the widths dependence on the velocity is practically absent, the temperature profile asymmetry is not pronounced, the widths of the leading and rear fronts are close to each other and are determined by the dimensionless scale factor l :

$$r_\pm \approx 1/|\gamma_\pm| = 27l\,\text{cm}. \qquad (14)$$

Thus, at a copper layer thickness $L = 10\,\mu$ m the width of the fronts $r_\pm \approx 0.27$ cm.

In Fig. 3, we show the dependences of the leading ($r_- = 1/|\gamma_-|$) and rear ($r_+ = 1/|\gamma_+|$) fronts widths on the substrate temperature and on the layer thickness for the half-widths of the temperature profile for the case of balls. The gas temperature does not change, $T_g = 293$ K. It can be seen that as the substrate temperature increases, the stationary temperature profile does not catastrophically expand when radiation cooling is taken into account.

Solving the boundary problem for the steady temperature profile

The steady-state temperature profile is determined by solving the dimensional equation (5) or the dimensionless equation (9) with boundary conditions at the periphery. For the model of a transversely unbounded metal layer, the boundary condition is to approximate the temperature to the equilibrium value $T = T_0$ ($\Theta = 0$). More precise boundary conditions follow from the asymptotics of such an approximation given above, see formulas (10) and (11) for the rate $\gamma_\pm$ of temperature approximation to the equilibrium value.

Equations (5) and (9) are nonlinear second-order ordinary differential equations. To solve them, it is convenient to go to a system of two first-order differential equations, introducing the logarithmic derivative of the relative temperature deviation

$$\gamma(\Theta) = \Theta^{-1}(\chi)d\Theta/d\chi \qquad (15)$$

and the equation for its change

$$\Lambda(\Theta)\Theta^2\gamma\frac{d\gamma}{d\Theta} + \left[K(\Theta)\Theta^2 + \Lambda(\Theta)\Theta\right]\gamma^2 + v_s c_v \Theta\gamma + [1 - R(\Theta)]I_0(\chi) = 0. \qquad (16)$$

Asymptotically at $\chi \to \pm\infty$, the logarithmic derivative $\gamma(\Theta)$ approaches values $\gamma_\pm$.

The dependence of the laser intensity profile can be approximated by a series of steps, at each of which the intensity is constant, $I_0 = \text{const}$. Within such a step, equation (16) will allow to find $\gamma(\Theta)$, and by stitching together solutions for different steps the complete dependence of this quantity over the entire range of variation. After determining $\gamma(\Theta)$, the coordinate relationship $\Theta(\chi)$ is found from the following inverse relationship from equation (15) $\chi = \int \frac{d\Theta}{\Theta\gamma(\Theta)}$. Practically, the numerical solution is carried out by the shotgun method of starting with the asymptotic at one edge of the temperature profile and selecting conditions to ensure that the correct asymptotic is achieved at the other profile edge.

This approach is the easiest to implement for very narrow (delta-shaped) laser beams and for a beam with an intensity profile in the form of a single step. In the first case, the $I_0(\chi)$ profile can be considered delta-shaped; the specific intensity profile is not important, and there is only one cross-linking boundary. In the second case, there are two cross-linking boundaries; the first case can also be considered a special case of the second, when simultaneously with decreasing step width (width of the laser beam), the maximum radiation intensity increases accordingly.

A comparison of the temperature profiles for laser beams with a stepped intensity profile of different widths at the same temperature at maximum is shown in Fig. 4. Recall that the dimensionless coordinate χ in Fig. 4 – 10 — is the dimensional coordinate normalized by

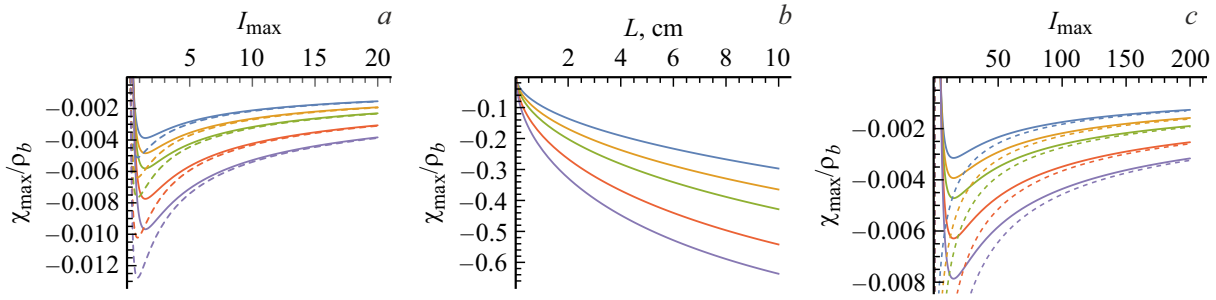

Figure 2. Dependence of the relative shift of the temperature profile maximum relative to the laser beam profile maximum on the plate thickness (b) and on the maximum intensity $I_{\max}$ [kW/cm ^{2}] for a given temperature at maximum $T_{\max} = T_{melt}/4 = 559$ K (a) and $T_{\max} = T_{melt} = 1356$ K (c), equal to the copper melting temperature. Substrate temperature $T_{\text{sub}} = T_g$. The different curves, from top to bottom, correspond to scanning speeds $V = 2, 2.5, 3, 4, 5$ cm/s. In the graphs, the beam width decreases with increasing $I_{\max}$ starting from $\rho_b = 1$, $r_b = 0.1$ cm at $I_{\max} = 2$ [kW/cm ^{2}] so that the power value $T_{\max} = T_{melt}/4 = 559$ K (a) or $I_{\max} = 6$ [kW/cm^2], at $P_{\text{in}} = 182$ W (c) is constant. The thickness of the ball layer is $L = 10\,\mu$ m. For thickness dependence (b) $I_{\max} = 20$ [kW/cm ^{2}]. Dotted curves — without regard to radiation cooling. Calculation for the example case of balls, $c_{\tau\text{eff}} = 400$, $c_{Sph} = 20$ and for accelerated heat transfer to the substrate, $c_{\text{subCu}} = 10$.

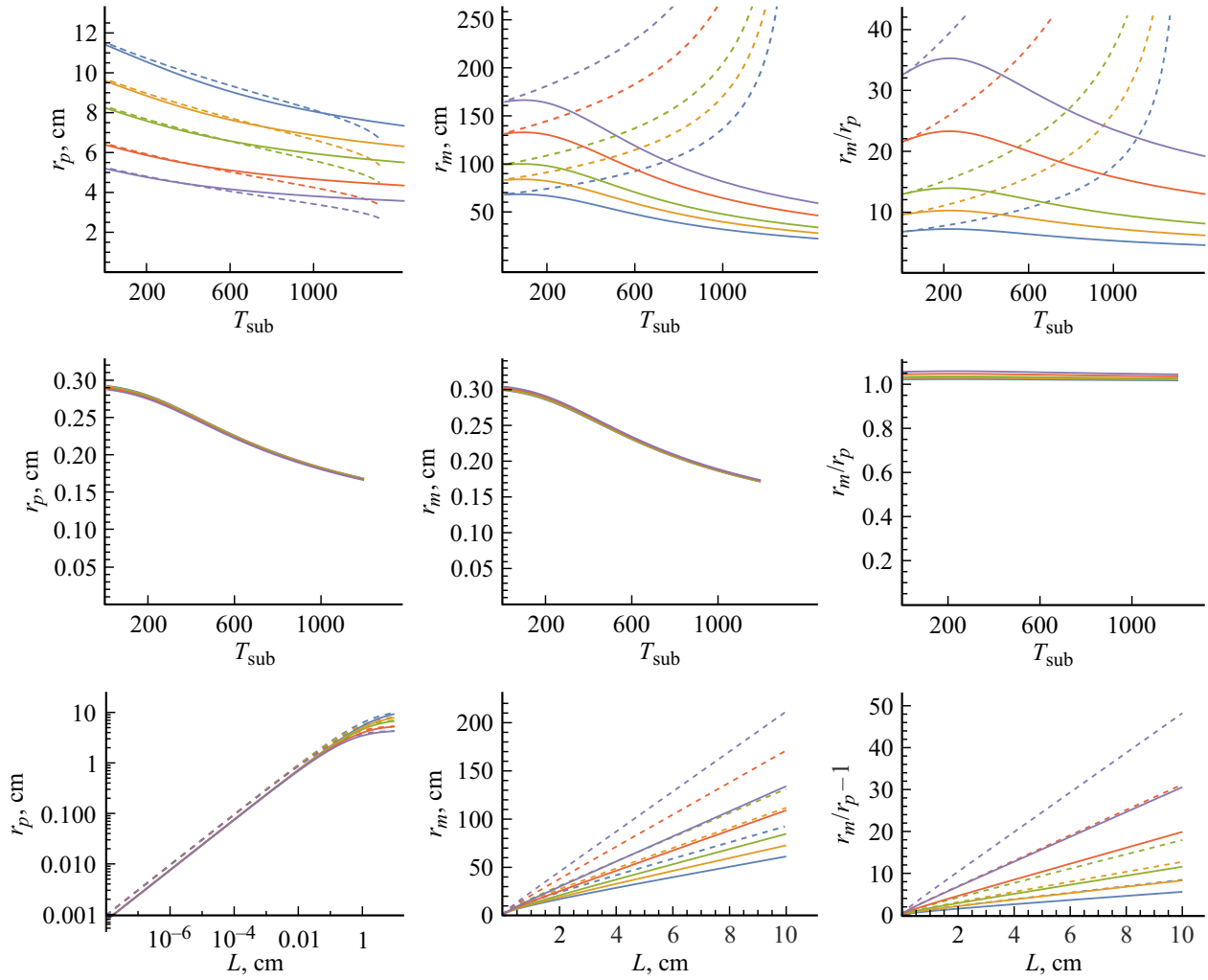

Figure 3. First and second row — dependences of the characteristic scale of the temperature profile decline at the leading and rear fronts, $r_{\pm}$, on the substrate temperature for different scanning speeds $V = 2$; 2.5; 3; 4 cm/s for curves r_- top down and $r_+, r_+/r_-$ bottom up, with layer thickness $L = 10$ cm in the first and $L = 10\,\mu$ m in the second row. Third row — dependences of the front widths on plate thickness L at $T_{\text{sub}} = T_g$. Calculation — for the example case of balls, $c_{\tau\text{eff}} = 400$, $c_{Sph} = 20$, and for accelerated heat transfer to the substrate, $c_{\text{subCu}} = 10$. The dashed curves — are for the case without regard to radiation cooling, i.e., with $\alpha_R = 0$.

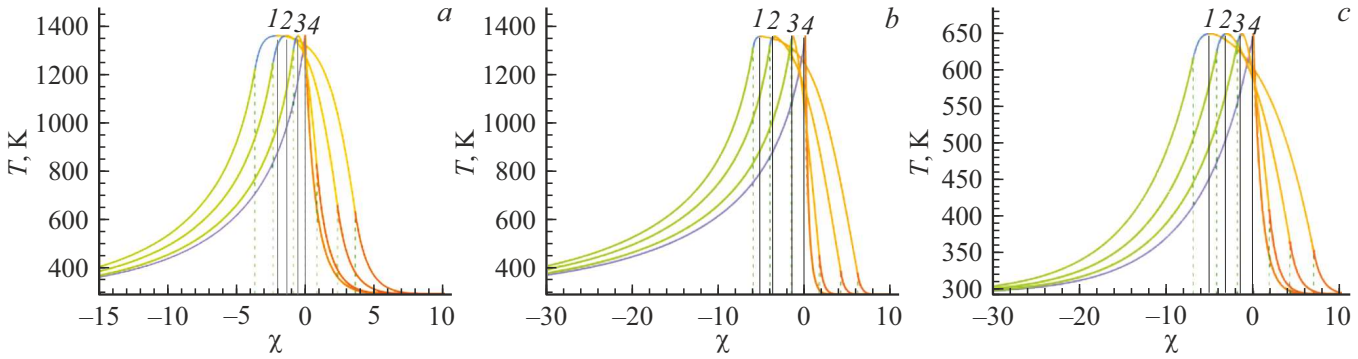

Figure 4. Temperature profiles for beams with staggered intensity profiles of different widths given the same maximum temperature, $T_m = T_{melt} = 1356$ (a, b) and $T_m = 647$ (c). The maximums of temperature profiles for different beams with a finite width are marked by a thin vertical line. The bundle boundaries are marked with strokes. The narrow beam center — at zero. Curves from left to right: beam half-width $\rho_b = 3.6, 2.35, 0.85, 0.0$, intensity $I_s = 5.16, 5.62, 9.38, \propto$ kW/cm ^{2}, power $P_b = 6.83,\ 3.1,\ 0.68,\ 1.0 \cdot l^2 \cdot$ MW (a) and $\rho_b = 6.07, 4.11, 1.63, 0.0$, $I_s = 5.16, 5.62, 9.38, \propto$ kW/cm^2, $P_b = 19.0,\ 9.52,\ 2.45,\ 1.8 \cdot l^2 \cdot$ MW (b), $\rho_b = 6.91, 4.21, 1.82, 0.0$, $I_s = 0.78, 0.93, 1.56, \propto$ kW/cm^2, $P_b = 3.73,\ 1.66,\ 0.52,\ 0.4 \cdot l^2 \cdot$ MW (c). Scan speed $V = 2 \cdot l^{-1}$ cm/s (a, c) and $5 \cdot l^{-1}$ cm/s (b). Parameters are chosen for the typical case of balls, $c_{\tau\,\mathrm{eff}} = 400$, $c_{Sph} = 20$ and for accelerated heat transfer to the substrate, $c_{\mathrm{subCu}} = 10$.

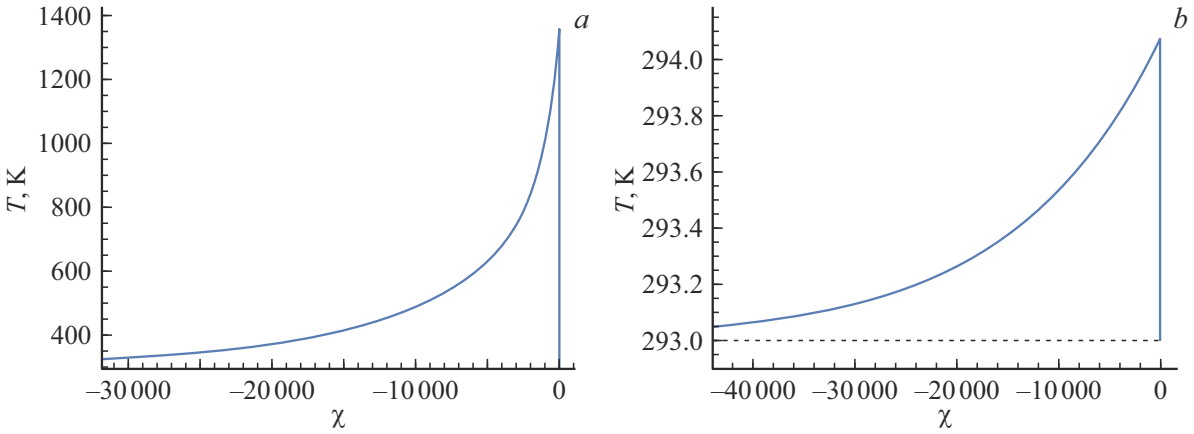

Figure 5. Temperature dependence on relative coordinate for high scanning speed, $V = c_{Sph} \cdot 5 \cdot l^{-1}$ cm/s (for ball layer $c_{\tau\,\mathrm{eff}} = 400$). (a) Dependence at power $P_{\mathrm{in}} = c_{Sph} \cdot 33 \cdot l^2 \cdot$ MW, when the temperature at maximum $T_{\max} = 1356$ K is slightly less than the copper melting temperature. (b) Dependence at $P_{\mathrm{in}} = c_{Sph} \cdot 53 \cdot l^2 \cdot$ kW, $T_{\max} = 294$ K, i.e. one degree above the ambient temperature, which is not enough to heat a$L = 10$ cm thick plate at this scan rate.

$(L \cdot \kappa_N/\alpha_{g,N})^{1/2}$ — a value proportional to the square root of the plate thickness L, and the dimensionless parameter $l = [L/(\kappa_N/\alpha_{g,N})]^{1/2}$ is also proportional to the root of L. It can be seen that the temperature maximum shift is greater, the smaller the beam intensity and the greater its width. For a wide beam with a maximum intensity close to I_{hom}, the bias increases sharply, and the temperature profile becomes almost homogeneous.

Next, Fig. 5 −10 shows the results of calculating the temperature profile of the boundary problem (16) in the narrow beam limit. In this formulation, the correction factor $c_{\tau\,\mathrm{eff}}$ enters only into the scaling of the scan rate and c_{Sph} into the scaling of the beam power (hereafter $c_{Sph} = 20$). Using the dimensionless parameter introduced above allows scaling the results by varying the metal layer thickness, laser beam power, etc. Figs. 5−10 are given for a given dimensionless speed v_s, and the temperature profiles for the copper ball layer differ from the solid copper layer only by increasing the scanning speed at $c_{\tau\,\mathrm{eff}} = 400$. Figs. 5 and 6 correspond to the scanning speed for the solid plate at the lower limit of the selected speed interval $V = (5 \div 10) \cdot l^{-1}$ cm/s, respectively, for the ball layer, it is higher speed $V = 2000 \cdot l^{-1}$ cm/s, so that the plate has almost no time to warm up during scanning. On the contrary, the solid plate heats up almost to the melting temperature, because the cooling rate in this case is not high enough, and the profile establishing time is very long. The incident beam power varies in these figures in the range $P_{\mathrm{in}} = (10 \div 50) \cdot l^2 \cdot$ MW. As a result, the leading front of the profile is very sharp and the rear very long. It should be noted, that the velocity interval used for the demonstration here is increased a hundredfold for $l = 10^{-2}$, $L = 10\,\mu$m. If, however, we

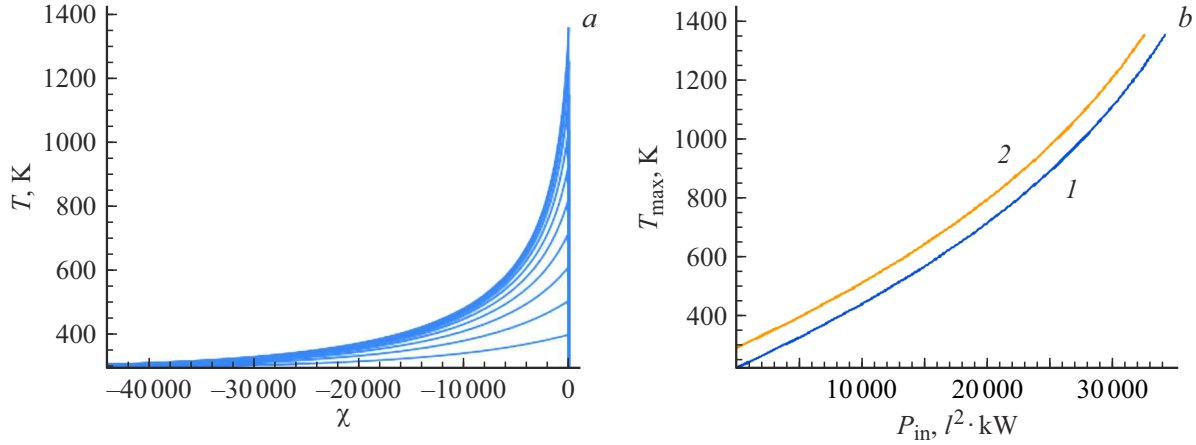

Figure 6. (*a*) Temperature dependence on relative coordinate for different beam powers, from $P_{in} = c_{Sph} \cdot 53 \cdot l^2 \cdot$ kW to $P_{in} = c_{Sph} \cdot 33 \cdot l^2 \cdot$ MW. Other parameters are the same, as in Fig. 5.(*b*) Temperature dependence at maximum on beam power in $[l^2 \cdot \text{kW}]$, i. e. the power on x axis varies from 5 to $30\,l^2 \cdot$ kW or for thin plate with $l = 0.01$, $L = 10\,\mu$ m, from 0.5 to 3 kW at high scan rate $V = c_{\tau\text{eff}} 5 \cdot l^{-1}$ cm/s. An additional curve *2* (yellow) is given for the cooled substrate, $T_{sub} = 202$ K.

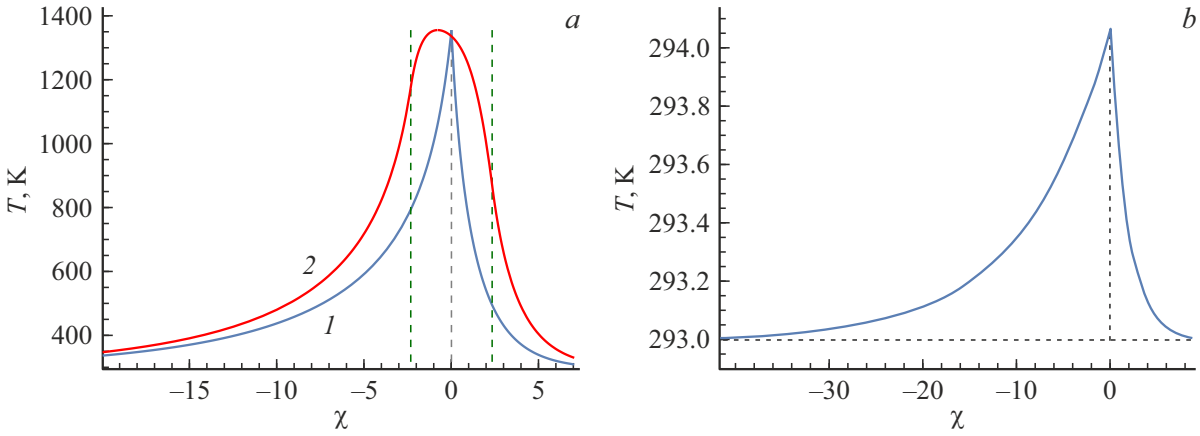

Figure 7. Temperature dependence on relative coordinate χ for small scanning speed, $V = l^{-1}$ cm/s in the case of balls at $c_{\tau\text{eff}} = 400$, $c_{\text{subCu}} = 10$, $T_{sub} = T_g = 293$ K. The position of the maximum of the steady-state temperature distribution is marked with strokes. (*a*) Graph for power $P_{in} = 792 \cdot l^2 \cdot$ kW, $T_{max} = 1396$ K. For (*b*) $P_{in} = 0.8 \cdot l^2 \cdot$ kW, $T_{max} = 294$ K, which is not enough to heat a plate thickness at this scan rate. The curve it 2 corresponds to the temperature profile for a stepped laser beam with a half-width of $\rho_b = 3$at the same temperature at maximum. The beam boundaries and center are indicated by vertical dashed lines. Maximum offset $\chi_m = -0.8$. Intensity across the beam width $I_s = 4.9$ kW/cm^2, power is the same, $P_{in} = 792 \cdot l^2 \cdot$ kW. Other parameters are the same, as in Fig. 5.

choose an $V = (5 \div 10)$ velocity interval of cm/s for such micron-sized layers, the temperature profile asymmetry will be significantly smaller, i.e., almost as in the following Figs. 9 and 10.

Figs. 7 and 8 correspond to the scanning speed $V = 10 \cdot l^{-1}$ cm/s for the ball layer. In this case, the balls are heated significantly for $P_{in} \sim 400 \cdot l^2 \cdot$ KW powers, but the length of the leading front of the temperature profile is only 10 times shorter than the rear front. In Figs. 9 and 10, the scanning speed is very low, so that the temperature profile is almost symmetrical. Both types of copper layers heat up significantly when the laser irradiation power is $P_{in} \sim 400 \cdot l^2 \cdot$ KW.

Fig. 11, *a* shows the general trends of the maximum temperature dependence on the scanning speed and beam power (in $[l^2 \cdot \text{kW}]$). Naturally, the scanning speed increase weakens the layer heating. Fig. 11, *b* shows the extent to which the laser power should be increased or the scanning speed decreased to achieve a particular maximum temperature. In a slightly different form, the same trend is shown in Fig. 11, *c*.

Conclusion

The analysis of the heating mode of the metal layer by a scanning laser beam leads to the following main conclusions.

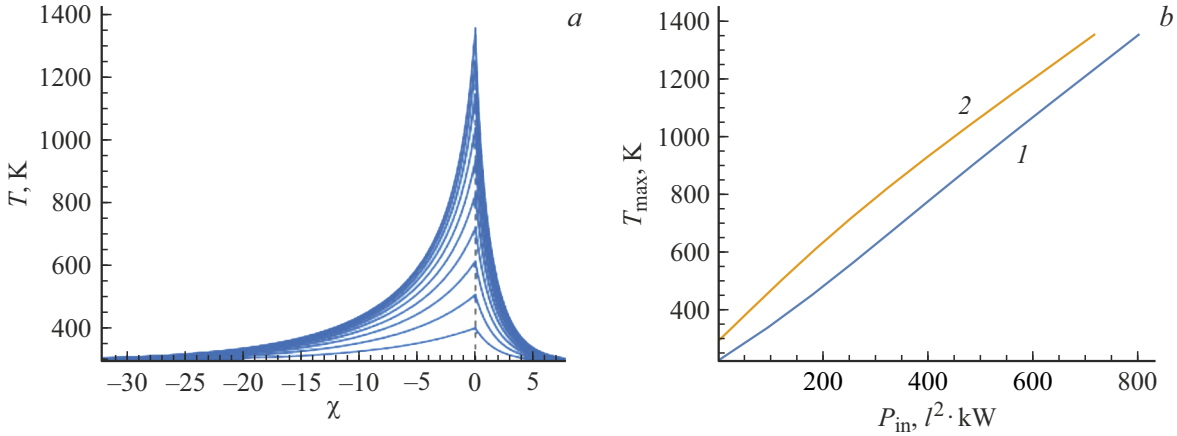

Figure 8. (*a*) Temperature dependence on relative coordinate for different beam powers, from $P_{\text{in}} = 0.8 \cdot l^2 \cdot \text{kW}$ to $P_{\text{in}} = 792 \cdot l^2 \cdot \text{kW}$. (*b*) Temperature dependence at maximum on beam power in $[l^2 \cdot \text{kW}]$ for small scan rate, $V = l^{-1}$ cm/s, curve *1*. An additional curve *2* is given for the cooled substrate, $T_{\text{sub}} = 178\,\text{K}$.

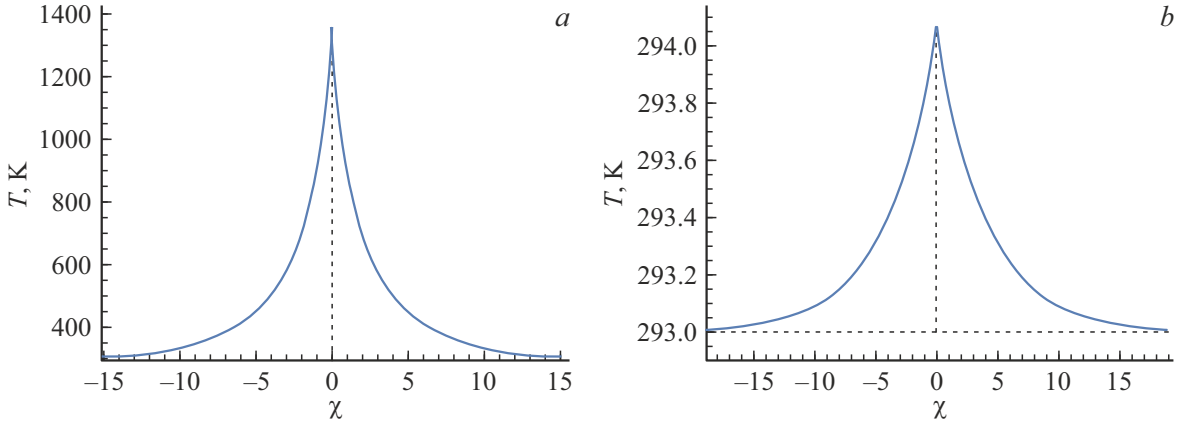

Figure 9. Temperature dependence on relative coordinate χ for low scanning speed, $V = 5 \cdot l^{-1}\,\mu$ m/s, for ball layer $c_{\text{reff}} = 400$. (*a*) Dependence at power $P_{\text{in}} = 719 \cdot l^2 \cdot \text{kW}$, $T_{\max} = 1356\,\text{K}$. (*b*) Dependence at $P_{\text{in}} = 0.61 \cdot l^2 \cdot \text{kW}$, $T_{\max} = 294\,\text{K}$, which is not enough to heat a plate of thickness $L = 10\,\text{cm}$. Other parameters are the same, as in Fig. 5. That is, the scanning speed in Figs. 7 and 8 almost does not change the magnitude of the heating power, but affects only the beam symmetry, leading to a relatively long rear front of the stationary profile.

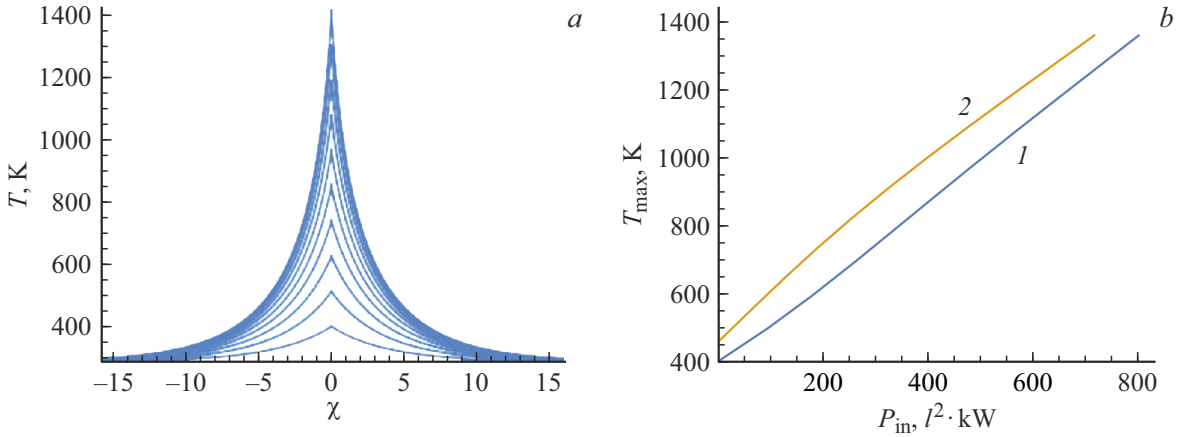

Figure 10. To the left — the temperature dependence on the relative coordinate for different beam powers, from $P_{\text{in}} = 0.61 \cdot l^2 \cdot \text{kW}$ to $P_{\text{in}} = 719 \cdot l^2 \cdot \text{kW}$. To the right — temperature dependence at maximum on beam power in $[l^2 \cdot \text{kW}]$ for near-zero scan rate, $V = 5 \cdot l^{-1}\,\mu$ m/s, curve *1*. An additional curve *2* is given for the cooled substrate, $T_{\text{sub}} = 202\,\text{K}$.

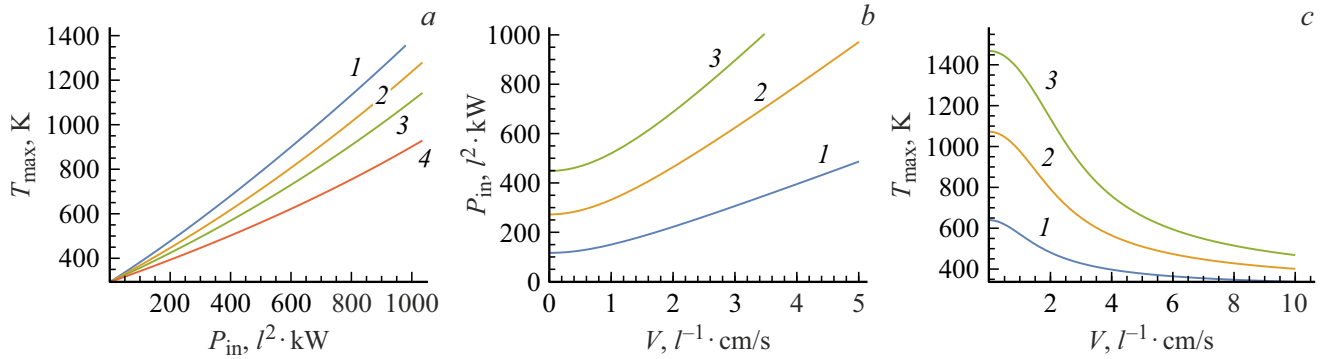

Figure 11. (a) Maximum temperature dependence for different scanning speeds, $V = 2; 2.5; 3; 4 \cdot l^{-1}$ cm/s for top-down curves (from blue to red), on laser power P [$l^2 \cdot$ kW].(b) Dependence of the laser power required to reach the maximum temperature $T_{max} = 500, 750, 100$ K for the bottom-up curves (from blue to green), on the scanning speed V [l^{-1}cm/s]. (c) Dependence of maximum temperature for different incident beam powers: $P_{in} = 200, 500, 800 \cdot l^2 \cdot$ kW for bottom-up curves (blue to green), from scan speed V [l^{-1}cm/s].

The metal layer structure is extremely important. Taking into account that the layer is not continuous (homogeneous), but consists of metal balls, changes the main characteristics of the mode by several orders of magnitude. In particularly, the temperature profile at a constant scanning speed of the laser beam is established in reasonable times practically only in the ball layer model.

Since, under characteristic conditions, the temperature profile width is noticeably greater than that of the laser beam, the beam shape has no significant effect on the heating characteristics. Sufficient information is given by considering the case of very narrow (delta-shaped) laser beams.

Taking into account the radiation heat transfer in the conditions where the metal layer temperature is close to the melting temperature, deterministically limits the temperature profile blurring.

The temperature profile maximum is shifted relative to the laser beam toward the rear front. The shift value becomes small for thin metal layers, see (13). The temperature profile asymmetry noticeably decreases with increasing scanning speed.

Funding

The study was supported by RFBR Grant No. 21-52-53009 GFEN.

Conflict of interest

The authors declare that they have no conflict of interest.

Appendix

Thermal-physical copper parameters

Here, we give values of parameters and coefficients in the dependences of thermal physical characteristics on temperature T, given in Kelvin, and their modification for the relative temperature $\theta = T/T_{work}$ in two operating ranges, $T_{work} = 293$ K and $T_{work} = 1300\,\text{K} < T_{melt} = 1356.55$ K, based on data [21–24]

Copper density: $\rho_0 = 8890$ [kg $\cdot$ m^{-3}],
$\rho_1 = 0.362$ [kg $\cdot$ m^{-3}K^{-1}],
$\rho(T) = 8890 - (8890 - 8680) \times (T - T_n)/(600 - 20)$ for $T_n = 293$ K, $\rho(T) = \rho_0 + \rho_1(T - T_n) = \rho_0[1 + \rho_\theta^{(1)}(\theta - \theta_n)]$,
$\rho_\theta^{(1)} = 0.012(0.0529)$ for $T_{work} = 293(1300)$ K.

Heat capacity: $c_p = 0.381$ [kJ/(kg $\cdot$ K)],
$c_v^{(1)} = 1.419 \cdot 10^{-4}$ [kJ/(kg $\cdot$ K^2)],
$c_v(T) = 0.374 + (0.414 - 0.374)(T - T_n)/(573 - 293)$,
$c_v = c_p/1.02 = 0.374$ [kJ/(kg $\cdot$ K)],
$c_v(T) = c_v + c_v^{(1)}(T - T_n) = c_v[1 + c_\theta^{(1)}(\theta - \theta_n)]$,
$c_\theta^{(1)} = 0.1115$.

Thermal conductivity coefficient:
$\kappa(T) = k(\theta) = \kappa_0 - \kappa_1 \cdot T + \kappa_2 \cdot T^2 - \kappa_3 \cdot T^3$,
$k_i = (-1)^i \kappa_i T_{work}^i$, $[k_j] = \text{Wm}^{-1}\text{K}^{-1}$, $\kappa_0 = 427$,
$\kappa_1 = 0.147$, $\kappa_2 = 1.14 \cdot 10^{-4}$, $\kappa_3 = 4.7 \cdot 10^{-8}$,
$[\kappa_j] = \text{Wm}^{-1}\text{K}^{-(j+1)}$. $k(\theta) = \kappa_0(1 + k_1\theta + k_2\theta^2 + k_3\theta^3)$,
$k_1 = -0.101$, $k_2 = 0.0229$, $k_3 = -0.00276$ for $T_{work} = 293$ K and $k_1 = -0.448$, $k_2 = 0.4508$, $k_3 = -0.241$ for $T_{work} = 1300$ K.

Convective (Newtonian) heat transfer:
Heat transfer with gas,
$\alpha_g(T) = h_0 - h_1 \cdot T + h_2 \cdot T^2 - h_3 \cdot T^3$,
$[c_v\rho_0] = \text{Jm}^{-3}\text{K}^{-1}$, $h_0 = 0$, $h_1 = 0.003$, $h_2 = 10^{-6}$, $h_3 = 10^{-9}$, $[h_j] = \text{Wm}^{-2}\text{K}^{-(j+1)}$, $[C_N] = \text{Wm}^{-2}\text{K}^{-1}$,
$c_N(T) = 1 + c_1 \cdot \theta + c_2 \cdot \theta^2 + c_3 \cdot \theta^3$, $c_1 = -0.11$, $c_2 = 0.0107$, $c_3 = -0.00314$ for $T_{work} = 293$ K, and $c_1 = -0.488$, $c_2 = 0.0475$, $c_3 = -0.0139$ for $T_{work} = 1300$ K. $c_N(T_{amb} = 293\,\text{K}) = 0.898$.
Heat exchange with a steel substrate $\alpha_{sub} = c_{sub\,Cu} C_{Fe} = \text{const}$, $C_{Fe} = 30$ [W m^{-2}K^{-1}].

Radiation heat transfer:
$\alpha_R = 4.54 \cdot 10^{-8}$ [W m^{-2}K^{-4}], $\beta_R = 0.143$.

Absorption coefficient: $1 - R(T) = B_0 b(\theta) = B_0 + {+}B_1 T + B_2 T^2$, $B_0 = 0.028$, $B_1 = 1.5 \cdot 10^{-5}$, $|B_2| \leq 10^{-8}$, $[B_j] = \mathrm{K}^{-j}$, $b(\theta) = 1 + b_1(\theta) + b_2(\theta)^2$, $b_1 = 0.157$, $|b_2| \leq 0.031$.

References

[1] A.A. Uglov, I.Yu. Smurov, A.M. Lashin, A.G. Guskov. *Modelirovaniye teplofizicheskikh protsessov impul'snogo lazernogo vozdeystviya na metally* (Nauka, M., 1991), (in Russian).

[2] A.M. Prokhorov, V.I. Konov, I. Ursu, I.N. Mihailescu. *Laser Heating of Metals* (CRC Press, Taylor & Francis Group, Boca Raton, FL, 1990).

[3] G.G. Gladush, I. Smurov. *Physics of Laser Material Processing. Theory and Experiment* (Springer-Verlag, Berlin Heidelberg, 2011).

[4] W.M. Steen, J. Mazumder. *Laser Material Processing. 4th Edition* (Springer, London, 2010).

[5] B.S. Yilbas, A.Y. Al-Dweik, N. Al-Aqeeli, H.M. Al-Qahtani. *Laser Pulse Heating of Surfaces and Thermal Stress Analysis* (Springer, Heidelberg, 2014).

[6] M. Gouge, P. Michaleris. *Thermo-Mechanical Modelling of Additive Manufacturing* (Elsevier Inc., Cambridge, MA, 2018).

[7] J.M. Dowden. *The Mathematics of Thermal Modeling. An Introduction to the Theory of Laser Material Processing* (Chapman & Hall/CRC, Boca Raton, FL, 2001).

[8] Seok Kim, Do Hyeog Kim, Wonpyo Kim, Young Tae Cho, Nicholas X. Fang. International J. Precision Engineering and Manufacturing-Green Technology, **8**, 303–326 (2021). https://bmf3d.com/high-precision-micro-3d-printers/

[9] J. Liu, Y. Zhou, S. Li, S. Wen, Q. Wei, C. Yan, Y. Shi. J. Alloys and Compounds, **688**, 626–636 (2016).

[10] T. Bhardwaj, M. Shukla. Materials Science and Engineering A, **734**, 102–109 (2018).

[11] Y. Yang, J.B. Zhan, Z.Z. Sun, H.L. Wang, J.X. Lin, Y.J. Liu, L.C. Zhang. J. Alloys and Compounds, **804**, 220–229 (2019).

[12] R. Esmaeilizadeh, A. Keshavarzkermani, U. Ali, Y. Mahmoodkhani, B. Behravesh, H. Jahed, A. Bonakdar, E. Toyserkani. J. Alloys and Compounds, **812**, 152097 (2020).

[13] W. Guo, B. Feng, Y. Yang, Y. Ren, Y. Liu, H. Yang, Q. Yang, L. Cui, X. Tong, S. Hao. Materials and Design, **215**, 110460 (2022).

[14] A. Collazo, R. Figueroa, C. Pérez, X.R. Nóvoa. Materials, **15**, 1353 (2022).

[15] B.B. Ravichander, K. Mamidi, V. Rajendran, B. Farhang, A. Ganesh-Ram, M. Hanumantha, N. Shayesteh Moghaddam, A. Amerinatanzi. Materials Characterization, **186**, 111765 (2022).

[16] S. Zou, Z. Zhao, W. Xu, X. Ni, L. Zhang, W. Wu, D. Kong, X. He, L. Wang, C. Dong. Optics and Laser Technology, **147**, 107652 (2022).

[17] R. Li, W. Yuan, H. Yue, Y. Zhu. Optics and Laser Technology, **146**, 107574 (2022).

[18] A. Mussatto, R. Groarke, R.K. Vijayaraghavan, M.A. Obeidi, P.J. McNally, V. Nicolosi, Y. Delaure, D. Brabazon. J. Materials Research and Technology, **18**, 2672–2698 (2022).

[19] N.N. Rozanov. Sov. Phys. JETP, **53**, 47 (1981).

[20] N.N. Rosanov. *Spatial Hysteresis and Optical Patterns* (Springer, Berlin, 2002).

[21] Thermalinfo.ru URL: http://thermalinfo.ru/svojstva-materialov/metally-i-splavy/svojstva- medi-plotnost-teploemkost-teploprovodnost

[22] V.E. Zinoviev. *Teplofizicheskie svoistva metallov pri vysokikh temperaturakh*, (Metallurgiya, M., 1989). (in Russian). http://thermalinfo.ru/spravochniki-skachat/zinovev-teplofizicheskie-svojstva-metallov-pri-vysokih-temperaturah; https://metallplaza.ru/cu/phispropcu.htm http://thermalinfo.ru/Sets/bibl_files/Zinovjev_teplofizicheskie_svoistva_metallov.djvu

[23] V.S. Chirkin. *Teplofizicheskie svojstva materialov yadernoj tekhniki. Spravochnik* (Atomizdat, M 1968). (in Russian). http://thermalinfo.ru/spravochniki-skachat/chirkin-spravochnik- po-teplofizicheskim-svojstvam-materialov-yadernoj-tehniki; http://thermalinfo.ru/Sets/bibl_files/chirkin-teplofizicheskie-svoistva-materialov-yadernoy-tekchniki-spravochnik.djvu

[24] Copper. URL: Incorrect Source Link

Translated by Y.Deineka